

# FINITE ELEMENT ANALYSIS OF CONCRETE CONE FAILURE MECHANISM IN POST-INSTALLED ANCHORS APPLIED TO FROST-DAMAGED CONCRETE

YUTARO ISHIDA<sup>\*</sup>, YUYA TAKASE<sup>†</sup>, TAITO SHIOKOSHI<sup>†</sup>,  
TSUTOMU ISHIGAKI<sup>††</sup> AND MUNEOMI TAKAHASHI<sup>††</sup>

<sup>\*</sup> Research Institute of Technology, TOBISHIMA Corporation  
5472 Kimagase, Noda-shi, Chiba-ken, Japan  
e-mail: yuutarou\_ishida@tobishima.co.jp

<sup>†</sup> College of Design and Manufacturing Technology, Muroran Institute of Technology  
27-1 Mizumotocho, Muroran-shi, Hokkaido, Japan  
e-mail: y.takase@mmm.muroran-it.ac.jp, 23041041@mmm.muroran-it.ac.jp

<sup>††</sup> Marketing Division, Hilti Japan, Ltd.  
2-6-20 Chigasakiminami Tsuzuki-ku, Yokohama-shi, Kanagawa-ken, Japan  
e-mail: tsutomu.ishigaki@hilti.com, muneomi.takahashi@hilti.com

**Key words:** Finite Element Analysis, Post-installed Adhesive Anchor, Frost-damaged Concrete

**Abstract:** This study provides insights into the performance of post-installed anchors in deteriorated concrete. Post-installed anchors are commonly used in existing reinforced concrete buildings for seismic retrofitting and equipment installation. However, studies on the performance of these anchors in deteriorated concrete are limited. This study focuses on the tensile resistance performance of post-installed anchors in frost-damaged concrete. Nine test specimens were fabricated with varying degrees of frost damage deterioration. The results showed that as frost damage increased, the tensile strength decreased, particularly at a 60% deterioration level. Observations of concrete failure confirmed that the angle of the cone-failure surface decreased with increasing deterioration levels. A finite element model was developed to analyze the damage state inside the member, considering the reduction in the material properties of the concrete. The analysis revealed variations in the crack angles and initiation times depending on the degree of frost damage deterioration.

## 1 INTRODUCTION

Post-installed anchors are commonly used in existing reinforced concrete buildings for seismic retrofitting and equipment installation. In principle, for post-installed anchors to be securely anchored, the base concrete must be sound. Nevertheless, concrete deteriorates owing to various external factors, such as neutralization, salt damage, frost damage, and alkali-aggregate reactions. However, considering the long-term use of buildings, there are cases where post-installed anchors must be anchored, even in existing deteriorated

concrete. To date, few studies have been conducted on the structural performance of post-installed anchors in deteriorated concrete.

The tensile failure modes of post-installed anchors include anchor bolt yielding, adhesion failure, and concrete cone failure. In this study, the effect of concrete deterioration on the tensile resistance performance is analyzed through experiments with nine specimens and a two-dimensional finite element analysis that reproduces them, focusing on concrete cone failure, which is considered to have the greatest effect on concrete deterioration.

## 2 OUTLINE OF EXPERIMENT

### 2.1 Parameters of specimen

The parameters of the test specimen are listed in Table 1. The main parameter of the test specimens was the relative dynamic modulus of elasticity ( $DM$ ), which represents the degree of deterioration owing to frost damage, at a depth of 30 mm from the concrete surface.  $DM$  was set at three levels: 100%, 80%, and 60%, with a total of nine specimens, three for each level.

In this study, a simplified method using liquid nitrogen was employed to degrade concrete, as described below. Non-AE concrete with an inferior frost resistance was used as the concrete mixture, as listed in Table 2. The material properties of the concrete aged 176 days before freezing and thawing are listed in Table 3.

The diameter of the anchor bolt  $d_a$  was set as 16 mm, and the diameter of the concrete drilling  $\phi$  was set as 22 mm. The embedded length of the anchor bolt  $l_e$  was standardized to  $4.5d_a$  for all the specimens. The material properties of the anchor bolts are listed in Table 4.

An epoxy-based injectable adhesive was used for all the specimens. The material properties of the epoxy resins are listed in Table 5.

### 2.2 Details of specimens

Figure 1 shows the details of the test specimens. They were manufactured as 450 mm  $\times$  450 mm concrete blocks in accordance with EOTA guidelines [1], ensuring a region with a radius of at least twice the embedded length  $l_e$  to accommodate cone failure. Owing to the brittle nature of concrete cone failure, there were concerns regarding the cracking of concrete blocks around the perimeter during pull-out testing. To address this issue, the perimeters of the concrete blocks were restrained using reinforcing bars and grout.

As mentioned previously, the deterioration of the concrete surface was achieved using a method involving liquid nitrogen proposed by Miyoshi et al. [2]. The procedure began by spraying liquid nitrogen onto the concrete surface. Once the temperature reached

**Table 1:** Parameters of the specimen

Specimen	Type of adhesive	$DM$ [%]	$d_a$ [mm]	$\phi$ [mm]	$l_e$ [mm]
Ep-100-1	Epoxy resin	100	16	22	$4.5d_a$ (=72)
Ep-100-2					
Ep-100-3					
Ep-80-1		80			
Ep-80-2					
Ep-80-3					
Ep-60-1		60			
Ep-60-2					
Ep-60-3					

$DM$ : Relative dynamic modulus of elasticity,  $d_a$ : Diameter of the anchor bolt,  $\phi$ : Diameter of the concrete drilling,  $l_e$ : Embedded length of the anchor bolt

**Table 2:** Concrete mixture

$W/C$ [%]	$s/a$ [%]	Quantity of material per unit volume of concrete [kg/m <sup>3</sup> ]				Air [%]
		$W$	$C$	$S$	$G$	
69.3	48.6	187	270	880	944	1.3

$W/C$ : Water-cement ratio,  $s/a$ : Sand-total aggregate ratio,  $W$ : Water,  $C$ : Cement,  $S$ : Sand (Fine aggregate),  $G$ : Gravel (Coarse aggregate), Air: Air content

**Table 3:** Material properties of the concrete

$f_c$ [N/mm <sup>2</sup> ]	$E_c$ [N/mm <sup>2</sup> ]	$f_t$ [N/mm <sup>2</sup> ]
39.2	24,800	2.81

$f_c$ : Compressive strength,  $E_c$ : Young's modulus,  $f_t$ : Splitting tensile strength

**Table 4:** Material properties of the anchor bolt

$d_a$ [mm]	$f_y$ [N/mm <sup>2</sup> ]	$f_u$ [N/mm <sup>2</sup> ]	$E_s$ [N/mm <sup>2</sup> ]	$EL$ [%]
16	568	723	208,000	18.1

$d_a$ : Diameter,  $f_y$ : Yield strength,  $f_u$ : Ultimate tensile strength,  $E_s$ : Young's modulus,  $EL$ : Elongation

**Table 5:** Material properties of the epoxy resin

$f_{bc}$ [N/mm <sup>2</sup> ]	$E_b$ [N/mm <sup>2</sup> ]	$f_{bt}$ [N/mm <sup>2</sup> ]
228	3,670	50.8

$f_{bc}$ : Compressive strength,  $E_b$ : Young's modulus,  $f_{bt}$ : Tensile strength

approximately  $-25\text{ }^{\circ}\text{C}$ , the concrete was immersed in hot water and melted until it reached a temperature above  $20\text{ }^{\circ}\text{C}$ . Subsequently, the dynamic elastic modulus of concrete  $E_d$  was determined using ultrasonic testing. Finally, the specimens were immersed in water at room temperature for approximately 5 min to supply moisture to the deteriorated areas. The entire process comprised one cycle.

The propagation velocity of the ultrasonic waves  $V$  was measured at the positions indicated in Figure 2. The dynamic elastic modulus  $E_d$  was calculated using Equation (1), proposed by Ogata et al. [3]:

$$E_d = 4.938V^2 + 14.438V + 20.708 \quad (1)$$

where  $E_d$  is the relative dynamic modulus [ $\text{N}/\text{mm}^2$ ], and  $V$  is the propagation velocity of the ultrasonic waves [ $\text{km}/\text{s}$ ].

Examples of the temperature history and variation in  $DM$  are shown in Figures 3 and 4, respectively. When  $DM=80\%$ , the target value for  $DM$  was reached between cycles 2 and 5. However, for  $DM=60\%$ , the target value was achieved between cycles 5 and 11. After the respective  $DM$  targets were reached in each case, concrete drilling was performed to install the anchor bolts.

### 2.3 Loading plan

The loading setup is illustrated in Figure 5. An unconfined testing method was adopted, and a center-hole hydraulic jack with a capacity of 320 kN was used to apply the tensile force. A pressure plate was installed between the hydraulic jack and the concrete face. The shape of the plate was based on EOTA [1], assuming a cone failure with an inner diameter of 320 mm, which was more than twice the embedded length of the anchor bolt  $l_e$ . In addition, No.7 silica sand was placed between the pressure plate and the concrete surface to prevent stress concentration caused by unevenness.

For the measurement of displacement, displacement gauges were placed at two points in the vertical direction at a height of 48 mm from the surface of the specimen. The average value was considered as the displacement  $S$  [mm] of the anchor bolt.

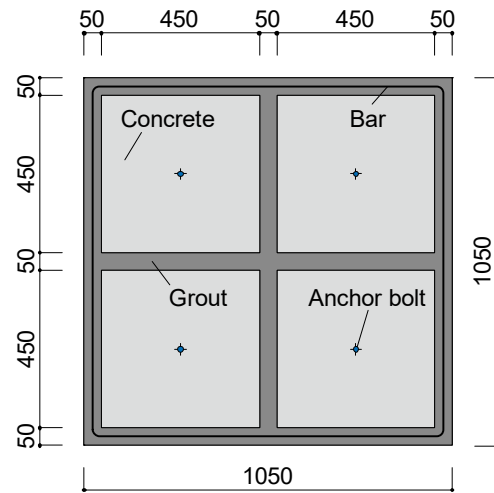


Figure 1: Details of the specimens

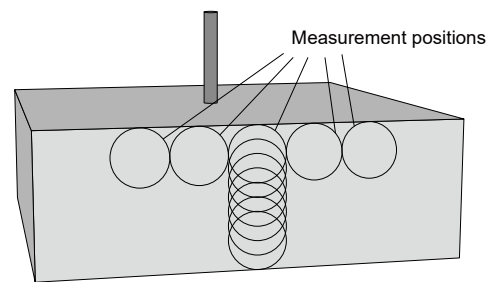


Figure 2: Measurement positions of ultrasonic waves

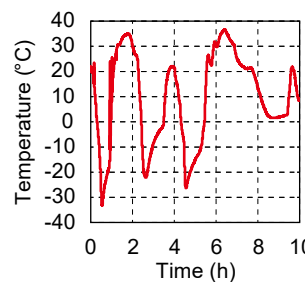


Figure 3: History of temperature

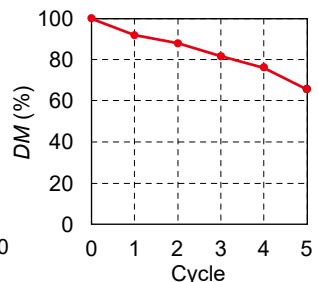


Figure 4: Variation of  $DM$

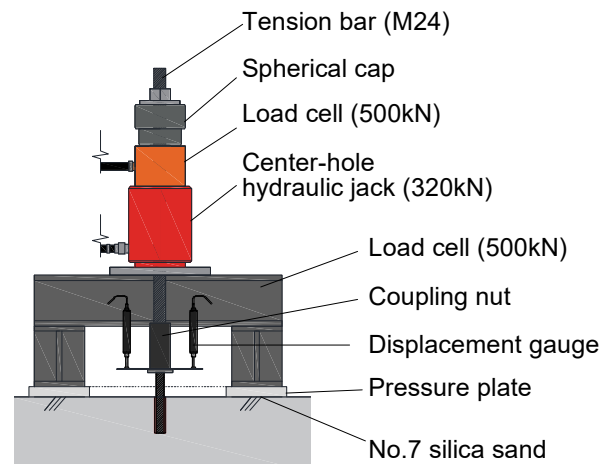


Figure 5: Loading setup (unconfined test)

### 3 EXPERIMENTAL RESULTS

#### 3.1 Load–displacement relationship

The load–displacement relationship in the pull-out experiments is shown in Figure 6. Note that, compared with Ep-100 series, Ep-80 series exhibited a reduction in strength of 3%–10%, whereas Ep-60 series showed a reduction of 7%–46%. In particularly, a significant decrease was observed in Ep-60 series.

When comparing the displacement at maximum load  $S_{max}$ ,  $S_{max}$  increased with the decrease in  $DM$ , indicating a larger displacement and a decrease in stiffness. Additionally, in some specimens, the load increased again after a decrease in load. This suggests the occurrence of complex failure mechanisms, such as concrete cracking (shear cracks or cone-shaped cracks), during the failure process.

#### 3.2 Correspondence with the evaluation equation

A comparison of the experimental and calculated values of tensile strength is presented in Table 6. According to the design formula of the Architectural Institute of Japan [4], the cone-failure strength of concrete was calculated using the following equation:

$$T_{cal} = 2/3 \cdot 0.31\sqrt{f'_c} \cdot A_c \quad (2)$$

where  $A_c$  represents the effective horizontal projection area.

The effective horizontal projection area  $A_c$ , which is determined by the failure angle, is important in the calculation of the cone-failure

strength of concrete. Here,  $A_c$  in Equation (2) was assumed to take the basic value of  $45^\circ$  and was calculated according to the following equation:

$$A_c = \pi \cdot l_e(l_e + d_a) \quad (3)$$

where  $l_e$  is the embedded length of the anchor bolt, and  $d_a$  is the diameter of the anchor bolt.

Furthermore, the reduction in the compressive strength of concrete owing to frost damage can be calculated using the following equation proposed by Suto et al. [5]:

$$f'_c = f_c \cdot \{0.0074 \cdot (DM - 100) + 1\} \quad (4)$$

The safety factor ( $T_{exp}/T_{cal}$ ) of the design tensile strength was observed to be 2.0 or higher for most of the test specimens. Although the values of some test specimens in the Ep-60 series fell below 2.0, they remained above 1.0.

**Table 6:** Experimental results and design strength

Specimen	$DM^*$ [%]	$T_{exp}$ [kN]	$S_{max}$ [mm]	$T_{cal}$ [kN]	$T_{exp}/T_{cal}$ [-]
Ep-100-1	-	61.2	0.71		2.38
Ep-100-2	-	51.5	0.47	25.8	2.00
Ep-100-3	-	57.3	0.52		2.22
Ep-80-1	84.9	54.8	1.06	24.3	2.26
Ep-80-2	83.5	54.9	0.89	24.1	2.27
Ep-80-3	83.5	51.2	0.69	24.1	2.12
Ep-60-1	67.9	40.0	2.69	22.5	1.78
Ep-60-2	58.8	52.7	0.95	21.5	2.45
Ep-60-3	65.6	31.9	0.99	22.2	1.43

$DM^*$ : Relative dynamic modulus of elasticity (real value),  $T_{exp}$ : Maximum tensile strength,  $S_{max}$ : Displacement at maximum tensile strength,  $T_{cal}$ : Design tensile strength

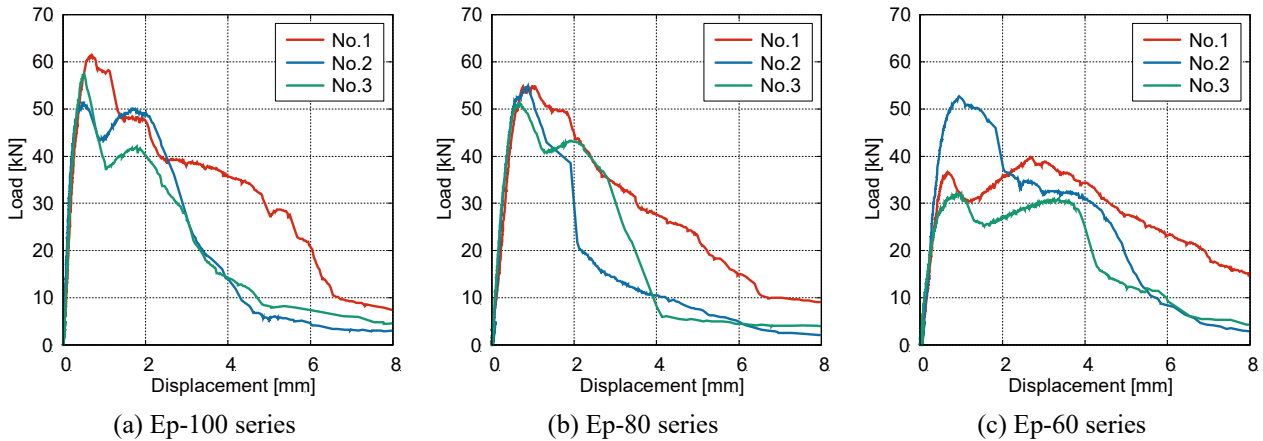


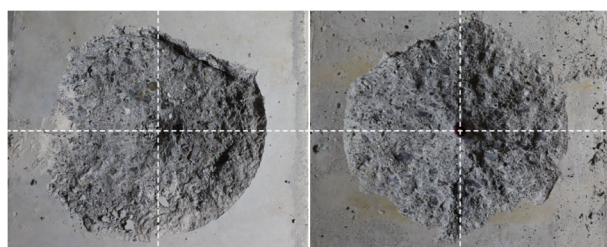
**Figure 6:** Load–displacement relationship

### 3.3 Failure state

Photo 1 shows the post-experimental failure conditions. After removing the cracked concrete and observing the final failure condition, it was observed that the concrete failure surface was on the inside of the pressure plate and formed from the lower part of the anchor bolt toward the pressure plate. Therefore, it can be concluded that the intended concrete cone failure is the primary failure mode.

Furthermore, as shown in Photo 2, the failure angle of each test specimen was measured using a replica gauge, and the corresponding values are listed in Table 7. The failure angle  $\theta$  exhibited a tendency to become more acute as  $DM$  decreased.

Based on the above observations, it can be



(a) Ep-100-3

(b) Ep-60-2

Photo 1: Failure state



(a) Ep-100-3

(b) Ep-60-2

Photo 2: Measurement of the failure angle

Table 7: Angle of the cone-failure surface

Specimen	$\theta_1$ [deg.]	$\theta_2$ [deg.]	$\theta_3$ [deg.]	$\theta_4$ [deg.]	$\theta_{ave.}$ [deg.]
Ep-100-1	66	72	68	66	
Ep-100-2	64	62	68	61	66
Ep-100-3	61	72	65	71	
Ep-80-1	65	63	66	59	
Ep-80-2	63	61	59	68	62
Ep-80-3	56	62	66	61	
Ep-60-1	59	75	45	58	
Ep-60-2	65	55	62	65	60
Ep-60-3	45	61	61	50	

$\theta_{1,4}$ : Failure angle at each direction,  $\theta_{ave.}$ : Average of failure angle

concluded that calculating the failure angle as  $45^\circ$  in the design equation is a conservative evaluation of the concrete failure surface, thereby ensuring a safety margin.

## 4 OUTLINE OF ANALYSIS

### 4.1 Configuration of the analysis model

An outline of the analytical model is shown in Figure 7. The analysis was conducted using the general-purpose nonlinear analysis software DIANA 10.5. The analysis was performed in two dimensions, and the concrete, anchor bolts, and epoxy resin were modeled using plane stress elements. Interface elements were inserted at the interface between the concrete and the epoxy resin, considering the adhesion property. The dimensions of each element were 2 mm.

The translational freedom in the Y-direction at the pressure plate, the translational freedom in the X-direction on both sides, and the rotational freedom in the Z-direction at the bottom surface were constrained. In addition, a forced displacement of up to 2 mm was applied to the top surface of the anchor bolt. The displacement increment was set as 0.02 mm.

Here, the cone-failure surface of the concrete is three-dimensional; however, in a two-dimensional model, the stress is averaged in the thickness direction. Therefore, when modeling in two dimensions, it is important to set the thickness of each element appropriately. As shown in Figure 8, the thickness of each element in this analysis model was set and converted into a two-dimensional representation.

For the concrete, considerations were made

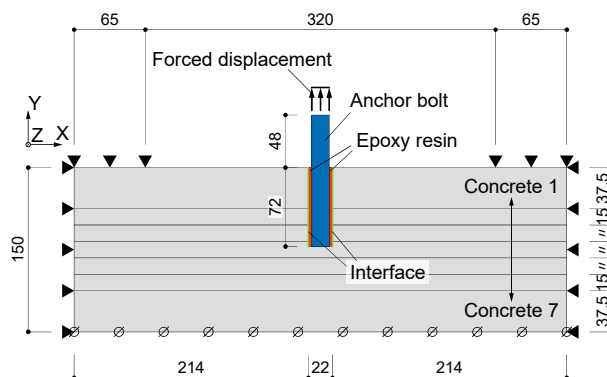
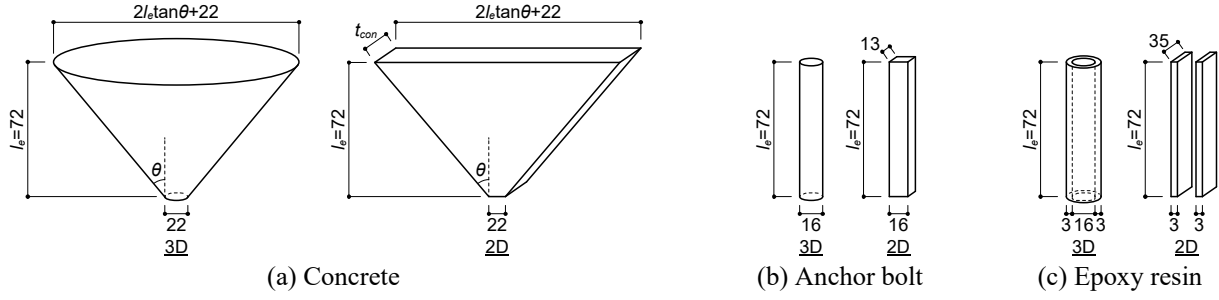


Figure 7: Outline of the finite element model


**Figure 8:** Configuration of each element (unit:[mm])

to ensure that the volumes of the cone-failure surfaces were equal. When the horizontal distance on the upper surface and height were set to the same values as in the three-dimensional case, the thickness  $t_{con}$  that resulted in equal volumes was calculated. Typically, the angle of the cone-failure surface was assumed to be  $45^\circ$ ; therefore,  $t_{con}$  was determined to be 88 mm.

A thickness of 13 mm was calculated for the anchor bolts to achieve the same volume as the cylindrical three-dimensional representation.

Efforts were made to ensure that the bonding area between the anchor bolt and the concrete was the same. The circumference of the adhesive with an outer diameter of 22 mm was calculated, and half that value, which was 35 mm, was considered the adhesive thickness.

## 4.2 Parameters of analysis model

The parameters of the analysis model are listed in Table 8. These parameters included the relative dynamic modulus and thickness of the concrete elements, and six cases were analyzed.

The deterioration of concrete was replicated according to the distribution of the damage mechanisms in terms of  $DM$  in the depth direction as listed in Table 9. The following equations, proposed by Suto et al. [5], were used to calculate the Young's modulus and tensile strength:

$$E'_c = E_c \cdot \{0.0014 \cdot (DM - 100) + 1\} \quad (5)$$

$$f'_t = f_t \cdot \{0.0074 \cdot (DM - 100) + 1\} \quad (6)$$

The strain at the compressive strength  $\varepsilon_c$  was calculated using the following equation proposed by Amemiya and Noguchi [6]:

**Table 8:** Parameters of the analysis model

Model	$DM$ [%]	$\theta$ [deg.]	$t_{con}$ [mm]
Ep-100-45	100		
Ep-80-45	80	45	88
Ep-60-45	60		
Ep-100-66	100	66	182
Ep-80-62	80	62	154
Ep-60-60	60	60	143

$t_{con}$ : Thickness of concrete elements

**Table 9:** Setting parameters of concrete

(a) Ep-100 series

No.	$DM$ [%]	$f_c$ [N/mm <sup>2</sup> ]	$E_c$ [N/mm <sup>2</sup> ]	$\varepsilon_c$ [ $\mu$ ]	$f_t$ [N/mm <sup>2</sup> ]	$G_F$ [N/mm]
-	100	39.2	24,800	2,238	2.81	0.0922

(b) Ep-80 series

No.	$DM$ [%]	$f'_c$ [N/mm <sup>2</sup> ]	$E'_c$ [N/mm <sup>2</sup> ]	$\varepsilon_c$ [ $\mu$ ]	$f'_t$ [N/mm <sup>2</sup> ]	$G_F$ [N/mm]
1	84.0	34.5	24,243	2,173	2.48	0.0884
2	92.4	37.0	24,535	2,207	2.65	0.0904
3	92.6	37.1	24,544	2,208	2.66	0.0905
4	92.1	36.9	24,527	2,206	2.65	0.0904
5	93.0	37.2	24,556	2,209	2.66	0.0906
6	93.9	37.4	24,589	2,213	2.68	0.0908
7	94.3	37.5	24,602	2,215	2.69	0.0909

(c) Ep-60 series

No.	$DM$ [%]	$f'_c$ [N/mm <sup>2</sup> ]	$E'_c$ [N/mm <sup>2</sup> ]	$\varepsilon_c$ [ $\mu$ ]	$f'_t$ [N/mm <sup>2</sup> ]	$G_F$ [N/mm]
1	64.1	28.8	23,554	2,092	2.06	0.0832
2	71.8	31.0	23,821	2,123	2.22	0.0853
3	76.8	32.5	23,996	2,144	2.33	0.0866
4	81.1	33.7	24,145	2,161	2.42	0.0877
5	83.8	34.5	24,236	2,172	2.47	0.0884
6	86.9	35.4	24,344	2,184	2.54	0.0891
7	89.7	36.2	24,441	2,196	2.60	0.0898

$f'_c$ : Reduced compressive strength,  $E'_c$ : Reduced Young's modulus,  $\varepsilon_c$ : Strain at compressive strength,  $f'_t$ : Splitting tensile strength,  $G_F$ : Fracture energy

$$\varepsilon_c = 13.97 \cdot f'_c + 1690 \quad (7)$$

The fracture energy of the concrete was calculated using the following equation proposed by the Japan Society of Civil Engineers [7]:

$$G_F = 10 \cdot (d_{max})^{1/3} \cdot f'_c{}^{1/3} / 1000 \quad (8)$$

where  $d_{max}$  represents the maximum aggregate size of the coarse aggregate in the concrete, which was 20 mm for the test specimens.

Subsequently, the thickness of the concrete element  $t_{con}$  was set to 88 mm based on the common assumption that the angle of the cone-failure surface is typically  $45^\circ$ , as mentioned earlier. However, considering that the actual failure angle was greater than  $45^\circ$ , those cases in which the calculation was based on the failure angle of each test specimen were included.

### 4.3 Material constitutive laws

The material constitutive laws for concrete are shown in Figure 9. The concrete was modeled using a fixed-crack model. The compressive side was modeled using the Naganuma-Ahamad model [8], whereas the tensile side was modeled using the model proposed by Hordijk et al. [9], which considers fracture energy. Furthermore, the shear stress transfer was assumed to be constant with a reduction factor of 0.01.

The material constitutive law for the anchor bolt is shown in Figure 10. The anchor bolt was modeled as a bi-linear model, and the von Mises yield criterion was adopted. However, the strain effects were not considered.

The epoxy resin was modeled as a linear elastic anisotropic model, as shown in Figure 11. The Young's modulus was set to  $3,670 \text{ N/mm}^2$ . In the shear direction, the shear deformation of the adhesive was considered in the joint element, as described later. Therefore, a large value of  $1.0 \times 10^6 \text{ N/mm}^2$  was set here for the shear elastic modulus to minimize the shear deformation.

### 4.4 Characteristics of joint element

Figure 12 illustrates the characteristics of the

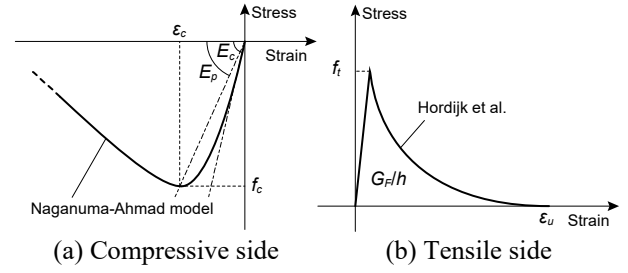


Figure 9: Material constitutive laws of the concrete

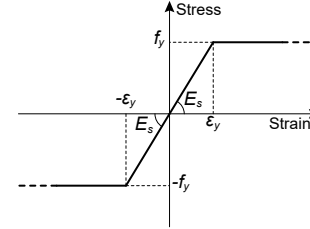


Figure 10: Material constitutive laws of the anchor bolt

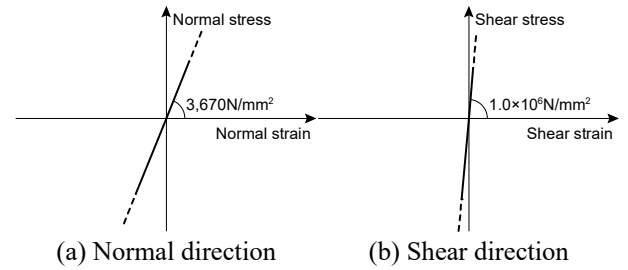


Figure 11: Material constitutive laws of the epoxy resin

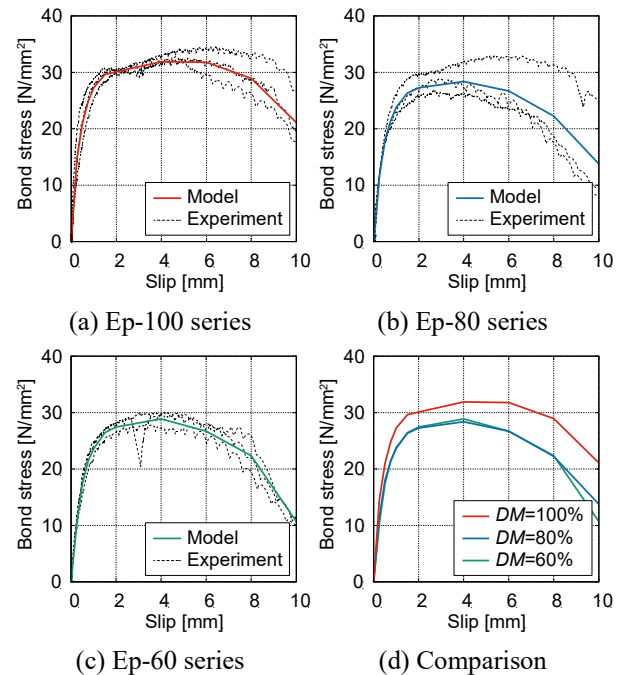


Figure 12: Characteristics of the joint element (interface between concrete and epoxy resin)

joint elements inserted between the concrete and the epoxy resin. The adhesion characteristics of the joint elements were determined from the adhesion test results of post-installed anchors in frost-damaged concrete conducted by Yano et al. [10].

On the other hand, a vertical stiffness of  $1.0 \times 10^6$  N/mm<sup>2</sup> was set to ensure adequate stress transmission.

## 5 ANALYSIS RESULTS AND DISCUSSION

### 5.1 Load–displacement relationship

The analysis results of the load–displacement relationship are shown in Figure 13.

First, focusing on the results of Ep-100-45, Ep-80-45, and Ep-60-45, where the angle of the cone-failure surface was assumed to be 45°, the results of all the analyses were much lower than those of the experimental results and had poor reproducibility. Furthermore, by comparing the analytical results of the three cases, the effect of frost damage on the reduction in stiffness and

maximum strength was observed to be negligible.

Subsequently, the results of the analyses of Ep-100-66, Ep-80-62, and Ep-60-60, which were prepared based on the cone-failure surface angles observed in the experiments, showed that the experimental results were generally reproduced with good accuracy. Similarly, a comparison of the analysis results for the three cases showed that the trends of decreasing stiffness and maximum strength with an increasing degree of frost damage deterioration were also reproduced.

In terms of the initial stiffness up to a displacement of 0.3 mm, the results for Ep-80-62 and Ep-60-60 were slightly larger than those of the experimental results, whereas Ep-100-66 reproduced the experimental results with high accuracy.

The maximum strength was generally consistent with the experimental results for all the cases. However, the displacements at the maximum strength tended to be slightly larger than those in the experimental results.

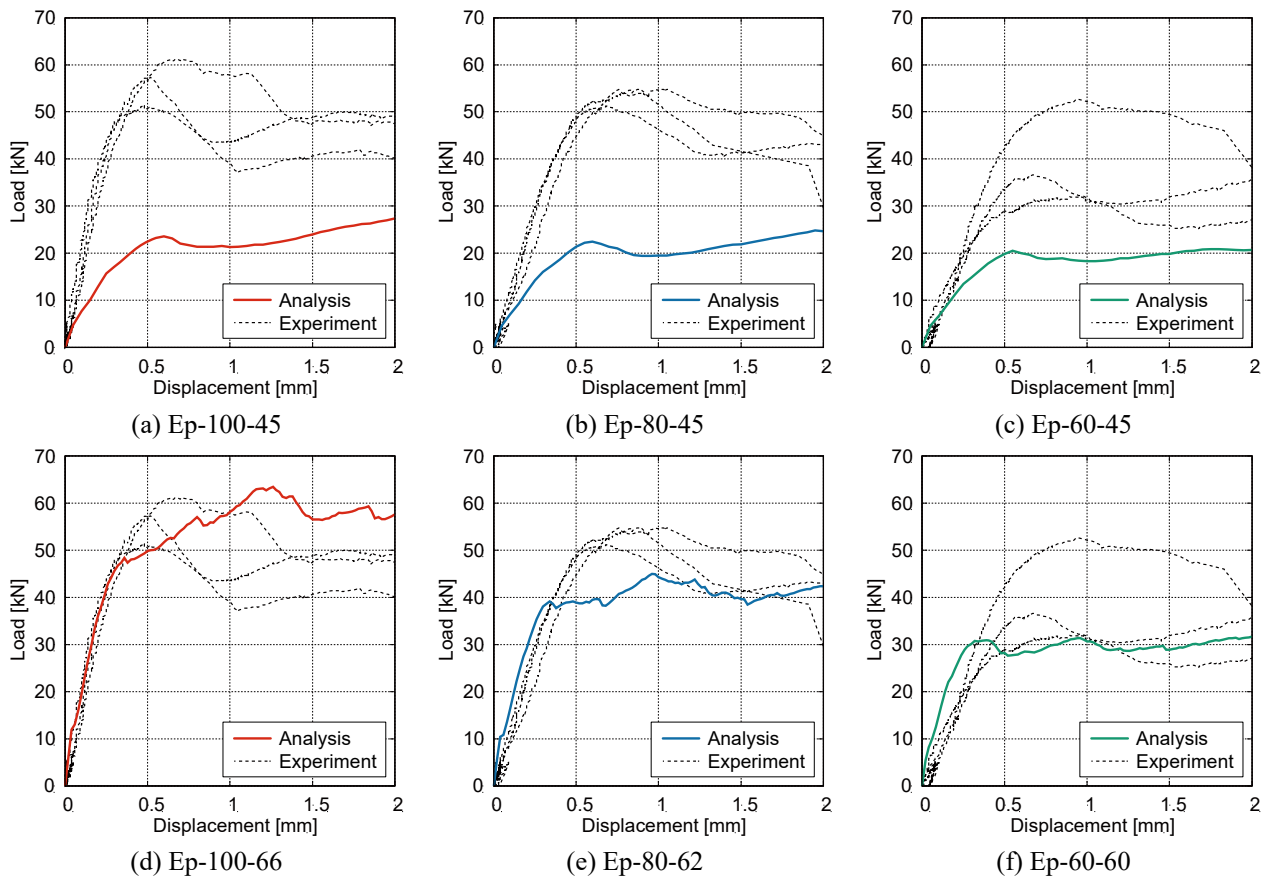


Figure 13: Load–displacement relationship

## 5.2 Crack strain distribution

The distribution of cracking strains for Ep-100-66, Ep-80-62, and Ep-60-60, extracted from the displacements in the range from 0 to 1 in increments of 0.2 mm, is shown in Figure 14. The maximum value of the crack strain and the angle of the assumed concrete failure surface are also provided in the figure.

As the frost damage degradation progressed, several cracks were observed in the vicinity of the anchor bolts when the displacement was small. Furthermore, the maximum value of the crack strain increased with the degree of frost deterioration. Therefore, it can be inferred that this is a factor in the decrease in stiffness as the degree of deterioration increases.

In addition, it was verified that the analytical results in terms of crack strain distribution and the experimentally observed cone-failure surface angles were mutually consistent.

Thus, the two-dimensional finite element model constructed in this study generally reproduced the experiments well.

## 6 CONCLUSIONS

In this study, experiments on the concrete cone failure of post-installed anchors in frost-damaged concrete were reproduced using two-dimensional finite element analysis. The results of the analysis were used to discuss the cone failure mechanism of frost-damaged concrete. The findings were as follows:

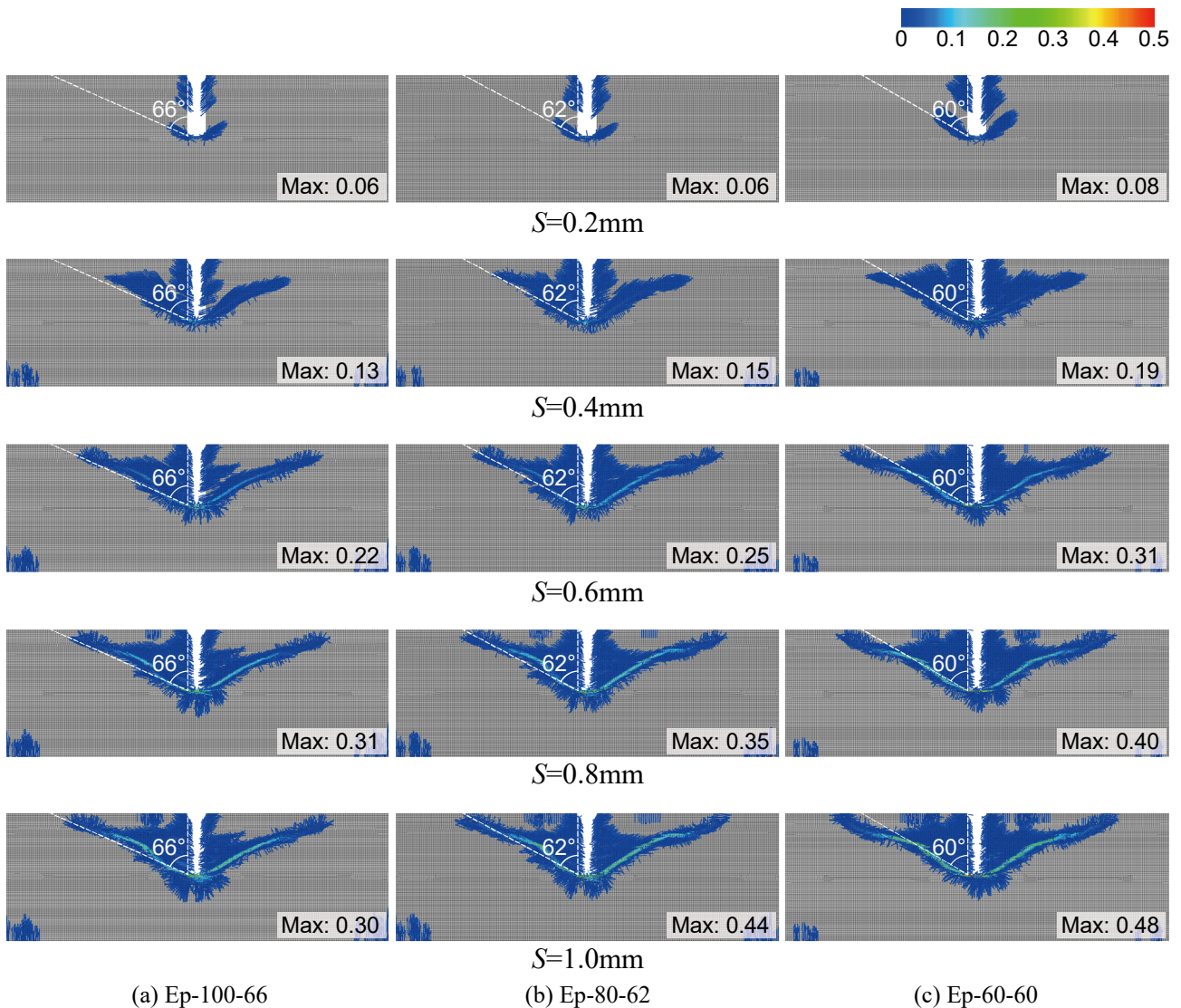


Figure 14: Crack strain distribution

- 1) The maximum strength and stiffness of concrete decreased as it deteriorated because of frost damage. Furthermore, the displacement at maximum strength increased.
- 2) In comparison with the design tensile strength according to the literature [1], it was observed that the safety factor exceeded 1, even for specimens with  $DM=60\%$ . This was because the angle of the cone-failure surface was estimated to be  $45^\circ$  in the design equation, whereas the actual failure angle was greater than  $60^\circ$ .
- 3) The model with a failure angle of  $45^\circ$  underestimated the experimental results and did not accurately reproduce the load–displacement relationship. However, the model with the actual angle of the cone-failure surface reproduced the results with good accuracy.
- 4) The results of the crack strain distribution analysis confirmed that they were generally consistent with the cone-failure surface angles observed in the experiments.
- 5) If the degree of deterioration was high, several cracks developed around the anchor bolts at the time of small deformations, and the maximum cracking strain was also higher. It was presumed that this caused a reduction in the stiffness and maximum strength.

## ACKNOWLEDGMENTS

This study was supported in part by the Japan Construction Anchors Association.

We also received significant contributions from Mr. Suenaga, a graduate of Muroran Institute of Technology; Mr. Yano, a graduate student at Muroran Institute of Technology; Dr. Ando, from Sumitomo Osaka Cement Co., Ltd.; and Dr. Abe, from Tobishima Corporation.

We sincerely appreciate their assistance and would like to acknowledge them here.

## REFERENCES

- [1] EOTA, 2018. EAD330499-01-0601: Bonded fasteners for use in concrete.
- [2] Miyoshi, K., Oikawa, Y., Yakase, Y. and Hama, Y., 2021. Fundamental Study on Bond Slip Between Repair Material and Frost-damaged Concrete. *Proceedings of the Concrete Structure Scenarios, JSMS*. **21**:544–549. (in Japanese)
- [3] Ogata, H., Hattori, K. and Takada, R., 2002. Evaluation of the freeze-thaw resistance of concrete by ultrasonic methods. *Proceedings of the Japan Concrete Institute*. **24**(1): 1563–1568. (in Japanese)
- [4] Architectural Institute of Japan, 2010. Design recommendations for composite constructions. (in Japanese)
- [5] Suto, M., Ogata, H., Ishigami, A. and Sato, S., 2016. Evaluation of Mechanical Properties and Dynamic Modulus of Elasticity by On-site Non-destructive Test in Deteriorated Concrete due to Frost Damage. *IDRE Journal*. **84**(3): I\_291–I\_299. (in Japanese)
- [6] Amemiya, A. and Noguchi, H., 1990. Development of finite element analytical program for high strength reinforced concrete members. Part 1. Development of concrete model. *Summaries of Technical Papers of Annual Meeting Architectural Institute of Japan*. **C-Structures 2**: 639–640. (in Japanese)
- [7] Japan Society of Civil Engineers, 2022. Standard Specifications for concrete structures, Design. (in Japanese)
- [8] Naganuma, K., Yonezawa, K., Kurimoto, O. and Eto, H., 2004. Simulation of nonlinear dynamic response of reinforced concrete scaled model using three-dimensional finite element method. *13<sup>th</sup> World conference on Earthquake Engineering. Paper no. 586*.
- [9] Hordijk, D.A., 1991. Local approach to fatigue of concrete. *PhD thesis, Delft University of Technology*.
- [10] Yano, Y., Takase, Y., Ishigaki, T. and Ishida, Y., 2023. Bond-slip property and strength estimation of various adhesive anchors to frozen damaged concrete. *Proceedings of the Japan Concrete Institute*. **45**(2): 907–912. (in Japanese)